JOURNAL OF INTEGRAL EQUATIONS
AND APPLICATIONS
Volume 30, Number 3, Fall 2018

NUMERICAL SOLUTIONS OF A CLASS OF SINGULAR NEUTRAL FUNCTIONAL DIFFERENTIAL EQUATIONS ON GRADED MESHES

PEDRO PEREZ-NAGERA AND JANOS TURI

ABSTRACT. In this paper, we present case studies to illustrate the dependence of the rate of convergence of numerical schemes for singular neutral equations (SNFDEs) on the particular mesh employed in the computation. In [**12**], a semigroup theoretical framework was used to show convergence of semi- and fully- discrete methods for a class of SNFDEs with weakly singular kernels. On the other hand, numerical experiments in [**12**] demonstrated a "degradation" of the expected rate of convergence when uniform meshes were considered. In particular, it was numerically observed that the degradation of the rate of convergence was related to the strength of the singularity in the kernel of the SNFDE. Following the idea used for Volterra equations with weakly singular kernels, see, e.g., [**1, 2**], we investigate graded meshes associated with the kernel of the SNFDE in attempting to restore convergence rates.

1. Introduction. Consider the following SNFDE in the state space $L^2_g(-r,0)$, a weighted L^2-space with kernel g:

$$\frac{d}{dt}\left(\int_{-r}^{0} g(\theta)x(t+\theta)\,d\theta\right) = f(t), \quad t>0,\ 0<r<\infty, \tag{1.1}$$

with initial condition

$$x(\theta)=\rho(\theta) \quad \text{for } -r\le\theta<0, \tag{1.2}$$

where ρ is in $L^2_g(-r,0)$. The kernel g appearing in (1.1) is positive and nondecreasing on $(-r,0)$ and weakly singular at zero. More precisely, $g(s)>0$ and $g'(s)\ge 0$ on $(-r,0)$ with $g(s)\to\infty$ as $s\to 0^-$ but still integrable, i.e., $g\in L^1(-r,0)$. It is helpful to keep in mind the so-called

2010 AMS *Mathematics subject classification.* Primary 34K28, 34K40, 65R20.
Keywords and phrases. Singular neutral equations, weakly singular kernels, graded meshes, rate of convergence.
Received by the editors on October 18, 2016, and in revised form on March 17, 2017.
DOI:10.1216/JIE-2018-30-3-447

Abel kernel $|s|^{-p}$ on $(-r, 0)$ with $0 < p < 1$, which represents a possible choice for g. The right-hand side function f is an integrable function. We note that an equation of this type occurs in certain aeroelastic systems, see **[3]**.

Using standard notation for neutral functional differential equations (NFDE), (1.1) could be rewritten as

$$\frac{d}{dt}Dx_t = f(t), \tag{1.3}$$

where the difference operator D is a bounded linear operator on $C := C([-r, 0]; \mathbb{R})$, the space of continuous functions on $[-r, 0]$, and x_t is the solution segment, i.e., $x_t(\theta) = x(t + \theta)$, $\theta \in [-r, 0]$. The neutral equation defined in (1.1)–(1.2) is called singular since its difference operator is not atomic at $s = 0$. Note that the difference operator D is said to be atomic at $s = 0$ if it has the representation

$$D\psi = \psi(0) + \int_{-r}^{0} \psi(s)\, d\mu(s)$$

for $\psi \in C$, where μ is a function of bounded variation on $[-r, 0]$ and such that

$$\lim_{\varepsilon \to 0} \mathrm{Var}_{[-\varepsilon, 0]}(\mu) = 0.$$

It was shown in **[4]** that atomicity of the D operator is a sufficient condition for well posedness of the NFDE on product spaces of the type $\mathbb{R} \times L^q([-r, 0]; \mathbb{R})$ for $q \geq 1$. In equation (1.1), consider the non-atomic D operator, defined by

$$D\psi := \int_{-r}^{0} \psi(s)|s|^{-p} ds,$$

with $0 < p < 1$ and $r > 0$. For this non-atomic operator, a well-posedness result was also obtained in **[4]** in product spaces under the assumption that $q < 1/(1 - p)$. Note that, for kernel singularity corresponding to $p = 1/2$, the implication is that we are not able use a Hilbert space setting ($q < 2$), which is very important for computational considerations. To remedy this, a weighted L^2-space was chosen and, in **[5, 12]**, it was shown that (1.1)–(1.2) is well posed on this state space, providing an opportunity to study convergence properties of numerical schemes in that setting. For a more in-depth

look at these issues, the reader is referred to **[4, 5, 11, 12, 14]**. Also, see **[10]** for a general discussion of NFDEs.

This paper is organized as follows. In Section 2, we introduce finite-dimensional approximations for the SNFDE (1.1)–(1.2). We also discuss graded discretizations of the interval $[-r, 0]$ in the construction of numerical schemes. In Section 3, we explore the degradation of the convergence rate in the scheme discussed in Section 2. In Section 4, case studies are presented to illustrate the dependence of the numerically observed rate of convergence on mesh selection. Concluding remarks may be found in Section 5.

2. Numerical approximations. In order to construct numerical schemes, we proceed as in **[12]** and convert the SNFDE (1.1)–(1.2) into a first order hyperbolic partial differential equation (PDE) with nonlocal boundary conditions. The initial data at $t = 0$ is given by the initial function $\rho(\theta)$, $-r \leq \theta \leq 0$, and the boundary is generated by the neutral equation itself.

Define $\varphi(t, \theta) := x(t + \theta)$ for $-r < \theta < 0$ and $t \geq 0$. Assuming that φ is differentiable, it satisfies the PDE:

$$\frac{\partial}{\partial t}\varphi(t, \theta) = \frac{\partial}{\partial \theta}\varphi(t, \theta), \tag{2.1}$$

for $t > 0$, $-r < \theta < 0$. Furthermore, it follows from (2.1) that the boundary condition for $t > 0$ can be written as

$$\int_{-r}^{0} g(\theta)\frac{\partial}{\partial \theta}\varphi(t, \theta)\, d\theta = f(t). \tag{2.2}$$

Remark 2.1. In the (t, θ)-plane, $\varphi(t, \theta)$ along $(0, \theta)$, $-r \leq \theta < 0$, is given by the initial condition $\rho(\theta)$. For $t > 0$, the right boundary, i.e., $\varphi(t, 0)$), can be obtained from (2.2), and then, $\varphi(t, \theta)$, $t > 0, -r \leq \theta < 0$ is determined along the characteristic lines. Using this perspective, other numerical schemes similar to that presented here may be constructed.

We begin by constructing the approximating function. Let N be a positive integer. We introduce the partition of the interval $[-r, 0]$ as

$$-r =: \tau_N^N < \tau_{N-1}^N < \cdots < \tau_1^N < \tau_0^N := 0,$$

and let $\delta_j^N := \tau_{j-1}^N - \tau_j^N > 0$ for $1 \le j \le N$. We define

$$\varphi^N(t,\theta) := \sum_{j=0}^{N} \alpha_j^N(t) B_j^N(\theta) \quad \text{for } t \ge 0,\ -r \le \theta \le 0,$$

where the piecewise linear functions, B_j^N, $j = 0, 1, 2, \dots, N$ are given as

$$B_j^N(\theta) := \begin{cases} (\theta - \tau_{j+1}^N)/\delta_{j+1}^N & \theta \in [\tau_{j+1}^N, \tau_j^N], \\ (\tau_{j-1}^N - \theta)/\delta_j^N & \theta \in [\tau_j^N, \tau_{j-1}^N], \\ 0 & \text{otherwise,} \end{cases} \quad \text{for } j = 1, 2, \dots, N-1;$$

$$B_0^N(\theta) := \begin{cases} (\theta - \tau_1^N)/\delta_1^N & \theta \in [\tau_1^N, \tau_0^N], \\ 0 & \text{otherwise;} \end{cases}$$

and

$$B_N^N(\theta) := \begin{cases} (\tau_{N-1}^N - \theta)/\delta_N^N & \theta \in [\tau_N^N, \tau_{N-1}^N], \\ 0 & \text{otherwise;} \end{cases}$$

and $\alpha_j^N(t)$, $j = 0, 1, 2, \dots, N$ are time-dependent coefficients. One option is to use uniform mesh in space, i.e., to select $\delta_j = \delta = r/N$. A more involved option is to use a graded mesh, that is, select δ_j, $j = 1, 2, \dots, N$ specifically for the particular SNFDE under consideration.

Graded meshes were applied in a collocation scheme in **[2]** to solve Volterra integral equations of the second kind with weakly singular kernels, and results on attainable optimal rates of convergence were given. In this paper, SNFDEs with weakly singular kernels are considered including kernels of the type $g(t) = t^{-p}$, with $0 < p < 1$, and thus, the results in **[2]** serve as a motivation to introduce graded meshes into the schemes presented here. In particular, we choose the mesh such that the area of the integral of the kernel of the SNFDE is the same on each subinterval, that is, we choose all τ_j^N such that

$$\int_{\tau_j^N}^{\tau_{j-1}^N} g(\theta)\, d\theta = \frac{1}{N} \int_{-r}^{0} g(\theta)\, d\theta \tag{2.3}$$

for $1 \le j \le N$ and where $g(\theta)$ is the kernel in equation (1.1). This mesh is applied for most examples in Section 4 (note that, in Example 4.6, it is somewhat modified to accommodate a more complicated kernel).

Throughout our computations, we use uniform time steps of size Δt on the interval $[0, T]$, where $T > 0$ denotes the final time. In order to simplify notation, the superscript N will be omitted during the remainder of this section.

Remark 2.2. While uniform meshes yield simpler schemes, especially when the space (δ) and time (Δt) discretization is selected such that $\delta = \Delta t$, their application leads to a degradation of the expected rate of convergence (see e.g., **[12]** for numerically observed rates of convergence). The numerical findings in **[12]** indicate that the degradation of the rate of convergence is directly related to the strength of the weak singularity in the kernel of the SNFDE. A dependence on the kernel singularity was also noted in **[8, 9]** in the context of numerical solutions of Abel integral equations, namely, convergence rates of $2-p$ were obtained for the kernels t^{-p}, $0 < p < 1$, when using a midpoint method with uniform mesh.

Motivated by the analysis in **[8]**, in this paper, rate of convergence estimates are presented for numerical schemes for SNFDEs (see Lemma 3.1 below). In particular, we arrive at a discretization error of order $2 - p$ in the uniform mesh case and order 2 in the graded mesh case, respectively, when we consider the difference of the integral in the boundary condition (2.2) and its fully discretized analog in equation (2.8). The numerical case studies in Section 4 indicate that the graded mesh (2.3) is a viable candidate to prevent the "degradation" of the expected convergence rate of 2 for the numerical schemes (2.9) for SNFDEs with more general weakly singular kernels as well.

See **[6, 7]** for related results on mesh selection. In **[6]**, an alternative method for solving a particular class of SNFDEs is given where the authors first convert the SNFDE to a Volterra equation of the second kind which is then solved using a hybrid collocation method.

Assume that a mesh is specified, and consider a second-order space discretization to equation (2.1) (see **[12]**):

$$\frac{d}{dt}\left(\frac{\alpha_{j-1}(t) + \alpha_j(t)}{2}\right) = \frac{1}{\delta_j}(\alpha_{j-1}(t) - \alpha_j(t)) \tag{2.4}$$

for $1 \le j \le N$, and substitute $\varphi(t, \theta)$ into the boundary condition (2.2)

to advance the solution to obtain

$$\sum_{j=1}^{N} \frac{g_j}{\delta_j}(\alpha_{j-1}(t) - \alpha_j(t)) = f(t), \tag{2.5}$$

where

$$g_j := \int_{\tau_j}^{\tau_{j-1}} g(\theta)\, d\theta.$$

Equations (2.4)–(2.5) form the semi-discrete scheme.

Using the second-order implicit trapezoidal rule in time in (2.4), we obtain the fully discretized scheme

$$\frac{1}{\Delta t}\left(\frac{\alpha_{j-1}^{k+1} + \alpha_j^{k+1}}{2} - \frac{\alpha_{j-1}^{k} + \alpha_j^{k}}{2}\right) = \frac{1}{2\delta_j}\left(\alpha_{j-1}^{k+1} - \alpha_j^{k+1} + \alpha_{j-1}^{k} - \alpha_j^{k}\right), \tag{2.6}$$

or, equivalently,

$$\alpha_{j-1}^{k+1} C_j + \alpha_j^{k+1} = \alpha_{j-1}^{k} + \alpha_j^{k} C_j, \tag{2.7}$$

where

$$C_j = \left(\frac{1}{\Delta t} - \frac{1}{\delta j}\right) \Big/ \left(\frac{1}{\Delta t} + \frac{1}{\delta j}\right).$$

The right boundary α_0^{k+1} is computed from the equation

$$\sum_{j=1}^{N} \frac{g_j}{\delta_j}(\alpha_{j-1}^{k+1} - \alpha_j^{k+1}) = f((k+1)\Delta t). \tag{2.8}$$

Since we are considering the second-order discretization (2.4) in space and the second-order discretization (2.6) in time for equation (2.1), it is reasonable to expect second-order convergence to the true solution. If the mesh is uniform, i.e., $\delta_j = \delta$, $j = 1, 2, \ldots$, and $\delta = \Delta t$, then $C_j = 0$ for all j. Thus, we obtain the particular scheme with uniform mesh considered in [**12**]. We now have a system of linear equations to determine α_j^{k+1}, $j = 0, 1, 2, \ldots, N$, namely,

$$\mathbf{K}_1 \mathbf{a}^{k+1} = \mathbf{K}_2 \mathbf{a}^{k} + \mathbf{F}^{k+1}, \tag{2.9}$$

$k \geq 0$, where

$$\mathbf{K}_1 := \begin{pmatrix} \frac{g_1}{\delta_1} & \left(\frac{g_2}{\delta_2} - \frac{g_1}{\delta_1}\right) & \cdots & \cdots & \left(\frac{g_N}{\delta_N} - \frac{g_{N-1}}{\delta_{N-1}}\right) & -\frac{g_N}{\delta_N} \\ C_1 & 1 & 0 & \cdots & 0 & 0 \\ 0 & C_2 & 1 & \cdots & 0 & 0 \\ \vdots & \vdots & \ddots & \ddots & 0 & 0 \\ 0 & 0 & \cdots & C_{N-1} & 1 & 0 \\ 0 & 0 & \cdots & 0 & C_N & 1 \end{pmatrix},$$

$$\mathbf{a}^k := \begin{pmatrix} \alpha_0^k \\ \alpha_1^k \\ \alpha_2^k \\ \vdots \\ \alpha_{N-1}^k \\ \alpha_N^k \end{pmatrix},$$

$$\mathbf{K}_2 := \begin{pmatrix} 0 & 0 & 0 & \cdots & 0 & 0 \\ 1 & C_1 & 0 & \cdots & 0 & 0 \\ 0 & 1 & C_2 & \cdots & 0 & 0 \\ \vdots & \vdots & \ddots & \ddots & 0 & 0 \\ 0 & 0 & \cdots & 1 & C_{N-1} & 0 \\ 0 & 0 & \cdots & 0 & 1 & C_N \end{pmatrix},$$

and

$$\mathbf{F}^k := \begin{pmatrix} f((k+1)\Delta t) \\ 0 \\ 0 \\ \vdots \\ 0 \\ 0 \end{pmatrix}.$$

Note that we have placed $\mathbf{F}^{k+1}$ on the right side of the equation since it is assumed to be a known quantity.

Remark 2.3. Note that the matrix $\mathbf{K}_1$ in (2.9) is nonsingular for all N for Abel-type kernels considered in the forthcoming examples.

Remark 2.4. The convergence of both the semi-discrete (2.4)–(2.5) and fully-discrete (2.7)–(2.8) schemes was established in **[12]**.

We now give a short explanation of system (2.9). At time $t = 0$, we have that $\alpha_j^0 = \rho(\tau_j)$ for $j = 1, \dots, N$ and α_0^0 can be computed from (2.8) (with $k = -1$). Thus, the vector $(\alpha_0^0, \alpha_1^0, \dots, \alpha_{N-1}^0, \alpha_N^0)^T$ is known and will be used to compute $(\alpha_0^1, \alpha_1^1, \dots, \alpha_{N-1}^1, \alpha_N^1)^T$. In a similar fashion, the vector of unknowns at step $(k+1)\Delta t$,

$$(\alpha_0^{k+1}, \alpha_1^{k+1}, \dots, \alpha_{N-1}^{k+1}, \alpha_N^{k+1})^T,$$

will be computed using

$$(\alpha_0^k, \alpha_1^k, \dots, \alpha_{N-1}^k, \alpha_N^k)^T$$

for all remaining $k \geq 1$. Assume that we are interested in approximating the true solution $x(k\Delta t)$ up unto time-step k_T. Then, the solution is approximated by $\phi^N(k\Delta t, 0)$ (since $\theta < 0$ introduces a delay), and thus, the numerical solution is continuously advanced by the α_0^k component (the right boundary mentioned above) in each newly computed vector up unto step k_T, that is, the numerical solution up unto time-step k_T is given by the values $\alpha_0^1, \alpha_0^2, \dots, \alpha_0^{k_T - 1}$ and $\alpha_0^{k_T}$.

In this section, a family of fully-discrete schemes with uniform and graded meshes was introduced for the numerical solution of SNFDEs with weakly singular kernels. In the next section, we establish error estimates for both cases for a special class of weakly singular kernels.

3. On the rate of convergence. Here, we provide an analysis of the discretization error of the integral in equation (2.2) and its fully disctretized analog in (2.8) for kernels of the type $g(\theta) = |\theta|^{-p}$, $0 < p < 1$, for uniform and graded meshes. Lemma 3.1 shows the superiority of the graded mesh (2.3) for these kernels.

Recall that the approximate solution is computed using the nonlocal boundary condition (2.2). For this reason, to study the convergence rate of the approximate solution to the true solution, we should understand how fast the fully-discretized version of the integral converges to the true value of the integral in (2.2). It is reasonable to expect that the global rate of convergence of the scheme would most likely benefit from a better approximation of the integral in (2.2), and therefore, we make

the characterization of this discretization error the main objective of this section.

At time $t_{k+1} > 0$, we want to establish a local consistency error bound between the integral

$$J := \int_{-r}^{0} g(\theta) \frac{\partial}{\partial \theta} \phi(t_{k+1}, \theta)\, d\theta$$

and its fully-discretized analog, given by

$$K := \sum_{j=1}^{N} \frac{g_j}{\delta_j} (\phi(t_{k+1}, \tau_{j-1}) - \phi(t_{k+1}, \tau_j)),$$

where ϕ is the true solution of (2.1)–(2.2). By a local consistency error, we mean how well the discretized version of the integral approximates the true integral. Consider a kernel g of the form $g(\theta) = |\theta|^{-p}$, and assume that $\phi(t_{k+1}, \cdot) \in C^3[-r, 0]$. The smoothness is assumed to accommodate a Taylor series approach for the error analysis.

We have the following result:

Lemma 3.1. *Let N be a positive integer, $t_{k+1} > 0$, $g(\theta) = |\theta|^{-p}$, $0 < p < 1$ for $\theta \in [-r, 0)$, $r > 0$, and assume that the solution of (2.1)–(2.2), $\phi(t_{k+1}, \cdot) \in C^3[-r, 0]$. Then, $J - K = O(N^{-(2-p)})$ with the uniform mesh, $\tau_j = -jr/N$, and $J - K = O(N^{-2})$ with the graded mesh generated by (2.3).*

Proof. We shall use the notation $\tau_{j/2} := (\tau_{j-1} + \tau_j)/2$. Define

$$K_j := \frac{g_j}{\delta_j} (\varphi(t_{k+1}, \tau_{j-1}) - \varphi(t_{k+1}, \tau_j))$$

and

$$J_j := \int_{\tau_j}^{\tau_{j-1}} g(\theta) \phi_\theta(t_{k+1}, \theta)\, d\theta,$$

$j = 1, 2, \ldots$, where we switched to the alternate notation $\phi_\theta = (\partial/\partial\theta)\phi$. Using straightforward calculations involving the Taylor series expansion of $\phi(t_{k+1}, \theta)$ with respect to its second argument around $\tau_{j/2}$, we obtain

the estimate

$$\left|\frac{1}{\delta_j}\left(\varphi(t_{k+1},\tau_{j-1})-\varphi(t_{k+1},\tau_j)\right)-\phi_\theta(t_{k+1},\tau_{j/2})\right|\le M\delta_j^2,$$

where $M:=\max_{[-r,0]}|\phi_{\theta\theta\theta}(t_{k+1},s)|$, and therefore, $|K_j-g_j\phi_\theta(t_{k+1},\tau_{j/2})|\le M\delta_j^2 g_j$. Using the Taylor expansion again around $\tau_{j/2}$, we have

$$\begin{aligned}
&J_j-g_j\phi_\theta(t_{k+1},\tau_{j/2})\\
&\quad=\int_{\tau_j}^{\tau_{j-1}}(-\theta)^{-p}\left(\phi_\theta(t_{k+1},\theta)-\phi_\theta(t_{k+1},\tau_{j/2})\right)\,d\theta\\
&\quad=\phi_{\theta\theta}(t_{k+1},\tau_{j/2})\int_{\tau_j}^{\tau_{j-1}}(-\theta)^{-p}\left(\theta-\tau_{j/2}\right)\,d\theta\\
&\qquad+\int_{\tau_j}^{\tau_{j-1}}(-\theta)^{-p}E(\theta)\,d\theta,
\end{aligned}$$

where $E(\theta)=(1/2)\phi_{\theta\theta\theta}(t_{k+1},\widetilde{\tau}_{j/2})(\theta-\tau_{j/2})^2$ is the error term, and $\widetilde{\tau}_{j/2}$ is between θ and $\tau_{j/2}$. From the mean value theorem for integrals, we have that

$$\left|\int_{\tau_j}^{\tau_{j-1}}(-\theta)^{-p}E(\theta)\,d\theta\right|=|E(\theta_j)g_i|\le M\delta_j^2 g_i,$$

where $\theta_j\in(\tau_j,\tau_{j-1})$. Denote $\xi_j=\tau_{j-1}/\delta_j$. In a fashion similar to Eggermont [**8**], using the change of variables $y=(\theta-\tau_{j-1})/(\tau_j-\tau_{j-1})$ and repeated integration-by-parts, we obtain that

$$\begin{aligned}
&\int_{\tau_j}^{\tau_{j-1}}\frac{(\theta-\tau_{j/2})}{(-\theta)^p}\,d\theta\\
&\quad=-\delta_j^{2-p}\int_0^1\frac{y-1/2}{(y-\xi_j)^p}\,dy\\
&\quad=\delta_j^{2-p}\left(\frac{p}{12}(1-\xi_j)^{-p-1}+\int_0^1 p(p+1)(y-\xi_j)^{-p-2}\left(\frac{y^3}{6}-\frac{y^2}{4}\right)dy\right)\\
&\quad=\delta_j^{2-p}O((1-\xi_j)^{-p-1})
\end{aligned}$$

as $-\xi_j\to\infty$. Combining the previous two estimates, we get

$$|J_j-g_j\phi_\theta(t_{k+1},\tau_{j/2})|\le C\delta_j^{2-p}(1-\xi_j)^{-p-1}+M\delta_j^2 g_i$$

for some constant C. Note that $J-K=\sum_{j=1}^{N} J_j-K_j$. Thus, denoting $h_j := g_j\phi_\theta(t_{k+1},\tau_{j/2})$, we obtain

(3.1)
$$|J-K| \le \sum_{j=1}^{N} |J_j-h_j|+|h_j-K_j| \le \sum_{j=1}^{N} C\delta_j^{2-p}(1-\xi_j)^{-p-1}+2M\delta_j^2 g_j.$$

If the mesh is uniform, then $\delta_j = r/N$ and $\tau_j = -rj/N$ for all j. This gives that $(1-\xi_j)^{-p-1} = j^{-p-1}$. Combining this with the fact that

$$\sum_{j=1}^{N} j^{-p-1} < \sum_{j=1}^{\infty} j^{-p-1} < \infty,$$

equation (3.1) gives that

$$\begin{aligned} |J-K| &\le 2Mr^2IN^{-2} + Cr^{2-p}N^{-(2-p)}\sum_{j=1}^{N} j^{-p-1} \\ &\le 2Mr^2IN^{-2} + C'N^{-(2-p)}, \end{aligned}$$

where C' is some constant and

$$I := \int_{-r}^{0} g(\theta)\,d\theta.$$

Thus, $J-K = O(N^{-(2-p)})$, if the mesh is uniform.

If the mesh is graded, then $g_j = I/N$ for all j. From this equation, we get that $\tau_j = -rj^{1/(1-p)}N^{-1/(1-p)}$. For $b > -1$ and $\nu \ge 1$, the inequality $(1+b)^\nu \ge 1+\nu b$ holds. Since $0 < 1-p < 1$, this inequality yields that

$$\left(1-\frac{1}{j}\right)^{1/(1-p)} \ge 1-\frac{1}{(1-p)j}.$$

From the inequality immediately above, we have that

(3.2)
$$\begin{aligned} \delta_j &= r\left(\frac{j}{N}\right)^{1/(1-p)}\left[1-\left(1-\frac{1}{j}\right)^{1/(1-p)}\right] \le r\left(\frac{j}{N}\right)^{1/(1-p)}\frac{1}{j(1-p)} \\ &= aj^{p/(1-p)}N^{-1/(1-p)} \\ &=: \Delta_j, \end{aligned}$$

where $a := r/(1-p)$. Note that $(1-\xi_j)^{-p-1} = \delta_j^{p+1}(-\tau_j)^{-p-1}$, and thus,

$$\begin{aligned}\delta_j^{2-p}(1-\xi_j)^{-p-1} &= \delta_j^3(-\tau_j)^{-p-1} \le \Delta_j^3(-\tau_j)^{-p-1} \\ &= a' N^{-2-(p/(1-p))} j^{-1+(p/(1-p))},\end{aligned} \tag{3.3}$$

where $a' := r^{2-p}/(1-p)^3$. Recall that

$$\sum_{j=1}^{N} j^q = O(N^{q+1})$$

for $q > -1$, and note that $\delta_j \le \Delta_j \le \Delta_N = aN^{-1}$. Hence, from equations (3.1), (3.2) and (3.3), we obtain that

$$\begin{aligned}|J-K| &\le 2MI\Delta_N^2 + Ca' N^{-2-(p/(1-p))} \sum_{j=1}^{N} j^{-1+(p/(1-p))} \\ &\le 2MIa^2 N^{-2} + C'' N^{-2-(p/(1-p))} N^{p/(1-p)}\end{aligned}$$

for some constant C''. Thus, $J-K = O(N^{-2})$ if the mesh is graded. □

Both claims in Lemma 3.1 are now established and show that the discretization error of $J-K$ converges to zero faster with the non-uniform graded mesh than with the uniform mesh. Note that we do not always have the smoothness assumption here; thus, the examples to follow will show that a discontinuity at zero in the derivatives of the true solution and the forcing function will also affect the rate of convergence. In addition, although we have only considered the case when $g(\theta) = |\theta|^{-p}$, it is believed that the graded mesh (2.3) improves the rate of convergence of the scheme even for more general kernels, e.g., g with the properties described in Section 1.

With Lemma 3.1 established, the question now is: how can the improvement in the discretization error $J-K$ affect the actual, i.e., numerically observed, rate of convergence of the numerical schemes (2.9)? The purpose of the next section is to give a partial answer to this question by presenting case studies to illustrate the dependence of the actual rate of convergence of the fully-discrete implicit scheme upon mesh selection.

4. Numerical examples. In this section, we consider examples where we apply the aforementioned scheme (2.9) using both uniform and graded meshes. We first give a few words on what we mean by numerical rate of convergence.

We want to study the rate of convergence of the error function $e_N(t) := \phi^N(t) - x(t)$ to zero, where t will be taken to be a time-step node point, that is, we want to estimate a value $m > 0$ such that $|e_N(t)| \le cN^{-m}$ as $N \to \infty$ and where $c > 0$ is a constant. Taking the logarithm of this inequality (assuming it is defined) we have

$$\log(|e_N(t)|) \le \log(c) - m\log(N) =: \ell(N).$$

We can see that $\log(e_N(t))$ lies below $\ell(N)$ for all N after some N' and, if we plot $\log(e_N(t))$ against $\log(N)$ (where $\log(N)$ is on the horizontal axis) as N increases, we can conclude that the sequence $\log(e_N(t))$ decreases at a rate m' that is at least as fast as m. We can then use m' as our approximate rate of convergence of $|e_N(t)|$ to zero. With this idea in mind, in the examples to follow, we will compute the approximate solution for $N = 10$, 20, 40, 80, 160 and 320 and plot the logarithm of the errors against the $\log(N)$ to approximate the rate of convergence. In Example 4.4, instead we consider the rate of convergence to zero of the maximum error

$$|e_N|_\infty := \max\{|e_N(t)| : t \in (0,1] \text{ is a time-step node point}\}$$

as N increases and apply this same idea.

When it is not apparent what the numerical rate of convergence is, e.g., see Figures 5–7 in Example 4.6, we provide least-squares lines to approximate the rate of convergence, that is, for fixed t, we provide a best fit function $ms + b$, where m and b are such that

$$\sum_{N \in A} [\log(e_N(t)) - (m\log(N) + b)]^2,$$

where $A := \{10,\ 20,\ 40,\ 80,\ 160,\ 320\}$, is minimized, i.e., m and b are such that $ms + b$ simultaneously minimizes the distance of each point $(\log(N), \log(e_N(t))$ to this line. This sum is a differentiable function of the two variables m and b and can, thus, be found using minimization techniques from standard calculus. A least-squares line will be considered to be the average numerical rate of convergence as the discretization in space is refined, and it will itself be referred to as

the numerical rate of convergence. These lines will be denoted as "– LS lines" in the figures.

Remark 4.1. In the examples to follow, we take a weakly singular Volterra equation of the first kind and reformulate it into an equation of the form (1.1). For example, consider an equation of the form:

$$\int_0^t g(t-s)x(s)\,ds = f(t), \tag{4.1}$$

where $f(0) = 0$, $f'(t)$ is locally integrable and x is the unknown function to be determined. Letting $\theta = -(t-s)$, we have that

$$\int_0^t g(t-s)x(s)\,ds = \int_{-t}^0 g(-\theta)x(t+\theta)\,d\theta,$$

and, in addition, if we define $x(u) = 0$ for $u \leq 0$, then (4.1) can be reformulated to take the form:

$$\frac{d}{dt}\left(\int_{-r}^0 g(-\theta)x(t+\theta)\,d\theta\right) = f'(t) \quad \text{for } t > 0,\ r > 0, \tag{4.2}$$
$$\text{with } x(\theta) = 0 \quad \text{for } -r \leq \theta \leq 0.$$

We shall use $T = 1$ and $r = 1$ in the examples to follow.

Example 4.2. Consider first this example, given in the text **[16]** on integral equations by Wazwaz,

$$\int_0^t \frac{x(s)}{(t-s)^{1/4}}\,ds = \frac{128}{231}t^{11/4}.$$

Reformulated, this equation can be stated as

$$\frac{d}{dt}\left(\int_{-1}^0 \frac{x(t+\theta)}{|\theta|^{1/4}}\,d\theta\right) = \frac{32}{21}t^{7/4}$$

for $t > 0$ and $x(t) = 0$ for $t \leq 0$. The solution is $x(t) = t^2$. The graded mesh is given by $\{\tau_j\}$, where

$$\int_{\tau_j}^{\tau_{j-1}} |\theta|^{-1/4}d\theta = \frac{1}{N}\int_{-1}^0 |\theta|^{-1/4}d\theta \tag{4.3}$$

for $j \geq 1$. In Figure 1, we plot $\log_2(e_N(t = 0.4))$ against $\log_2(N)$ with $\Delta t = 1/N$ as N increases. We see that the convergence rate at $t = 0.4$

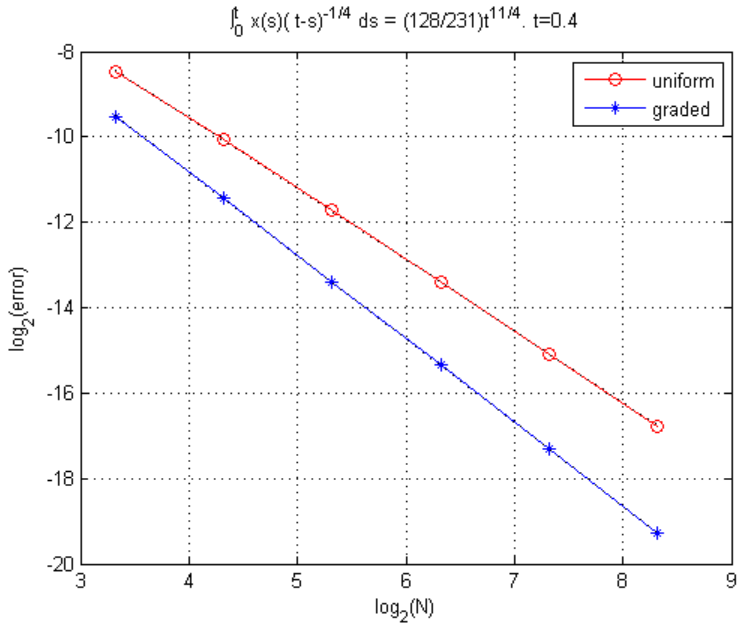

FIGURE 1. Example 4.2. Approximate rates of convergence for both meshes at $t = 0.4$.

TABLE 1. Example 4.2. Graded error table. $\Delta t = 1/N$.

mesh↓ time→	0.2	0.4	0.6	0.8
10	0.001013657	0.001353132	0.001610427	0.001854214
20	0.000272433	0.000357831	0.000423953	0.000479526
40	7.15E-05	9.33E-05	0.000110144	0.000124464
80	1.85E-05	2.41E-05	2.84E-05	3.20E-05
160	4.76E-06	6.16E-06	7.25E-06	8.17E-06
320	1.21E-06	1.57E-06	1.84E-06	2.08E-06

is approximately 1.9 for the graded mesh and approximately 1.6 for the uniform mesh. From Tables 1 and 2, we can see that accuracy is also better with graded mesh under most mesh sizes.

TABLE 2. Example 4.2. Uniform error table. $\Delta t = 1/N$.

mesh↓ time→	0.2	0.4	0.6	0.8
10	0.002077632	0.002830702	0.003326358	0.003706897
20	0.000707676	0.000926724	0.001072235	0.001184404
40	0.000231681	0.000296101	0.00033911	0.000372326
80	7.40E-05	9.31E-05	0.000105834	0.000115691
160	2.33E-05	2.89E-05	3.27E-05	3.56E-05
320	7.23E-06	8.91E-06	1.00E-05	1.09E-05

TABLE 3. Example 4.3. Graded error table. $\Delta t = 1/N$.

mesh↓ time→	0.2	0.4	0.6	0.8
10	0.000170697	0.001140789	0.003566658	0.008178993
20	4.40E-05	0.000287571	0.000895002	0.002046136
40	1.11E-05	7.20E-05	0.000223952	0.000511856
80	2.78E-06	1.80E-05	5.60E-05	0.000127977
160	6.95E-07	4.51E-06	1.40E-05	3.20E-05
320	1.74E-07	1.13E-06	3.50E-06	8.00E-06

Example 4.3. This example is given in **[15]**, where Rahman, et al., study numerical solutions of first and second kind weakly singular Volterra equations using Laguerre polynomials,

$$\int_0^t \frac{x(s)}{(t-s)^{1/2}}\, ds = t^5.$$

Reformulated, this equation can be stated as

$$\frac{d}{dt}\left(\int_{-1}^{0} \frac{x(t+\theta)}{|\theta|^{1/2}}\, d\theta \right) = 5t^4$$

for $t > 0$ and $x(t) = 0$ for $t \leq 0$. The solution is $x(t) = 1280/315\pi t^{9/2}$.

From Tables 3 and 4, we can see that accuracy is increased at most time-steps shown for the graded mesh. Furthermore, from Figure 2, we can also see that, at $t = 0.6$, the rate of convergence is ≈ 1.45 for uniform mesh and ≈ 2 for graded mesh.

TABLE 4. Example 4.3. Uniform error table. $\Delta t = 1/N$.

mesh↓ time→	0.2	0.4	0.6	0.8
10	0.000385704	0.003632379	0.01320325	0.032723612
20	0.00016053	0.001446193	0.00514585	0.012585171
40	6.39E-05	0.000556191	0.001947204	0.004715879
80	2.46E-05	0.000208414	0.000721241	0.00173485
160	9.21E-06	7.67E-05	0.000263218	0.000630195
320	3.39E-06	2.79E-05	9.51E-05	0.000226974

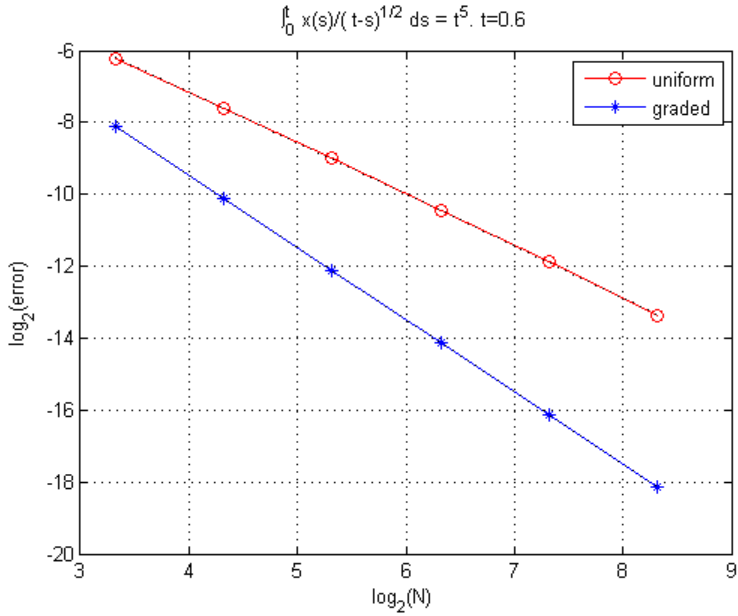

FIGURE 2. Example 4.3. Approximate rates of convergence for both meshes at $t = 0.6$.

Example 4.4. This example was also found in the text **[16]**. Consider

$$\int_0^t \frac{x(s)}{(t-s)^{1/2}}\,ds = \frac{8}{3}t^{3/2} + \frac{16}{5}t^{5/2}.$$

Reformulated, this equation can be stated as

$$\frac{d}{dt}\left(\int_{-1}^{0} \frac{x(t+\theta)}{|\theta|^{1/2}}\, d\theta\right) = 4t^{1/2} + 8t^{3/2}$$

for $t > 0$ and $x(t) = 0$ for $t \leq 0$. The solution is $x(t) = 2t + 3t^2$.

In this example, we look at the convergence to the solution in the max error $|e_N|_\infty$ as N increases. The max error was chosen here so that we can obtain an understanding of the error on the whole interval and not only at a fixed time. From Figure 3, we can estimate that the max error rate of convergence is ≈ 1.5 for both uniform and graded mesh with $\Delta t = 1/N$. Unlike the first two examples, note that the forcing function in the reformulated equation has an unbounded derivative at zero. It seems that this discontinuity may have compromised the expected rate of convergence of 2 for the graded mesh. From Tables 5–6, we can see that the accuracy appears to be better for the graded mesh.

TABLE 5. Example 4.4. Graded error table. $\Delta t = 1/N$.

mesh↓ time→	0.2	0.4	0.6	0.8
10	0.009505526	0.004760497	0.000962417	0.00126726
20	0.004514347	0.002602599	0.001423843	0.001190168
40	0.001852882	0.001142082	0.000758405	0.000998067
80	0.000711964	0.000457861	0.000329369	0.000379532
160	0.000264705	0.000175193	0.000131781	0.000138337
320	9.66E-05	6.52E-05	5.04E-05	4.77E-05

TABLE 6. Example 4.4. Uniform error table. $\Delta t = 1/N$.

mesh↓ time→	0.2	0.4	0.6	0.8
10	0.016568542	0.026032073	0.033280012	0.039371411
20	0.006508018	0.009842853	0.012389938	0.014532092
40	0.002460713	0.003633023	0.004529736	0.00528466
80	0.000908256	0.001321165	0.001637446	0.00190389
160	0.000330291	0.000475972	0.000587655	0.000681773
320	0.000118993	0.000170443	0.000209904	0.000243164

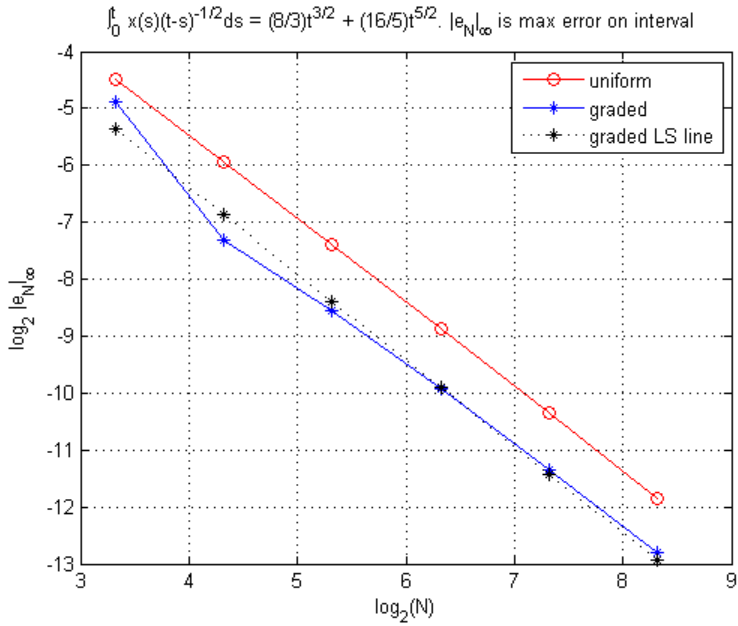

FIGURE 3. Example 4.4. Approximate rates of convergence in the max error on $(0, 1]$.

Example 4.5. This example was found in **[13]**, where Jahanshahi, et al., considered a numerical method to solve Abel integral equations of the first kind. Consider

$$\int_0^t \frac{x(t)}{(t-s)^{1/2}}\, ds = e^t - 1.$$

Reformulated, this equation can be stated as

$$\frac{d}{dt}\left(\int_{-1}^{0} \frac{x(t+\theta)}{|\theta|^{1/2}}\, d\theta \right) = e^t$$

for $t > 0$ and $x(t) = 0$ for $t \leq 0$. The solution is given by

$$x(t) = \frac{e^t}{\sqrt{\pi}}\, erf(\sqrt{t}),$$

where $erf(u) = 2/\sqrt{\pi} \int_0^u e^{-t^2} dt$ is the error function.

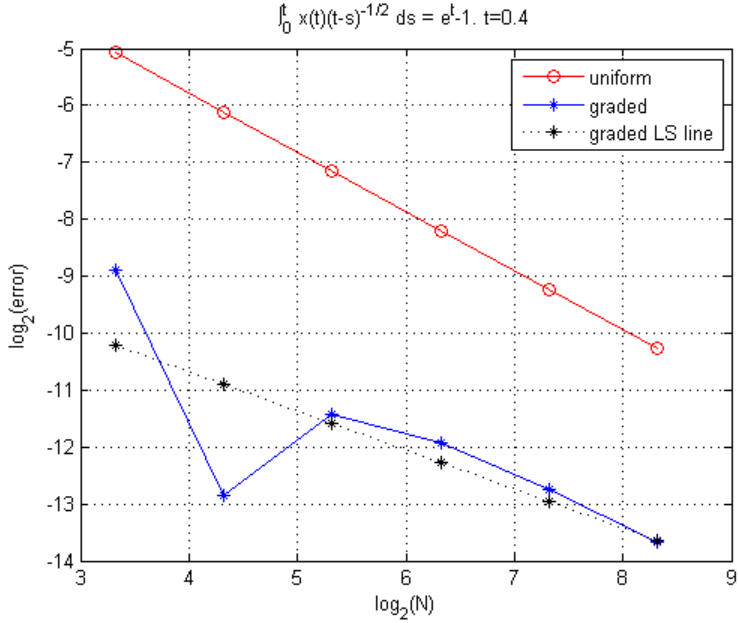

FIGURE 4. Example 4.5. Approximate rates of convergence for both meshes at $t = 0.4$.

At $t = 0.4$, Figure 4 shows that the uniform mesh and the graded mesh yield rates of convergence of approximately 1 and 0.66, respectively, for the given range of mesh sizes. These slow rates of convergence are not surprising since the solution has unbounded derivatives at zero. Figure 4 and Tables 7–8 show that there is a significant increase in accuracy with graded mesh.

Example 4.6. We now consider the next example, found in [**12**],

$$\frac{1}{\sqrt{\pi}} \int_0^t \frac{e^{-(t-s)}}{(t-s)^{1/2}} x(s)\, ds = e^{-t}(t + t^3 + t^5).$$

Reformulated, this equation can be stated as

$$\frac{d}{dt}\left(\int_{-1}^{0} \frac{e^{\theta}}{|\theta|^{1/2}} x(t+\theta)\, d\theta \right) = \sqrt{\pi}(-e^{-t}(t + t^3 + t^5) + e^{-t}(1 + 3t^2 + 5t^4))$$

TABLE 7. Example 4.5. Graded error table. $\Delta t = 1/N$.

mesh↓ time→	0.2	0.4	0.6	0.8
10	0.000370818	0.002113945	0.003781737	0.00386041
20	0.002143661	0.00013414	0.000542405	0.003049412
40	0.001550951	0.000363341	7.40E-06	0.000872734
80	0.000890558	0.000254809	6.73E-05	0.000370849
160	0.00047324	0.000145548	4.96E-05	0.000116045
320	0.000243497	7.73E-05	2.88E-05	8.89E-06

TABLE 8. Example 4.5. Uniform error table. $\Delta t = 1/N$.

mesh↓ time→	0.2	0.4	0.6	0.8
10	0.039093198	0.030079998	0.026815735	0.025626279
20	0.019228306	0.014461254	0.01263222	0.011821375
40	0.009444242	0.006989921	0.006006089	0.005521185
80	0.004651519	0.003401174	0.002884524	0.002613131
160	0.002298403	0.00166528	0.001398143	0.001252004
320	0.001138937	0.000819623	0.000682923	0.00060611

for $t > 0$ and $x(t) = 0$ for $t \leq 0$. The solution is given by

$$x(t) = e^{-t}\left(\frac{\Gamma(2)}{\Gamma(3/2)}t^{1/2} + \frac{\Gamma(4)}{\Gamma(7/2)}t^{5/2} + \frac{\Gamma(6)}{\Gamma(11/2)}t^{9/2}\right).$$

Note that the solution has unbounded derivatives at zero.

It is reasonable to expect the scheme to be more accurate as Δt gets smaller. Hence, the purpose of this example is to study how the rate of convergence at different times is affected when we consider time-steps smaller than $\Delta t = 1/N$. The size of system (2.9) does not change when we decrease the step-size since the discretization of $[-1, 0]$ remains fixed.

Note that the kernel gives difficulty in extracting a graded mesh tailored to this particular equation. Instead, we use the mesh we obtain by ignoring the exponential part, i.e., the mesh generated using kernel $g(\theta) = |\theta|^{-1/2}$, since the strength of the singularity at zero is similar for both kernels.

At $t = 0.2$, Figure 5 suggests that the rate of convergence is approximately 0.5 with $\Delta t = 1/N$, and, if we decrease the step-size

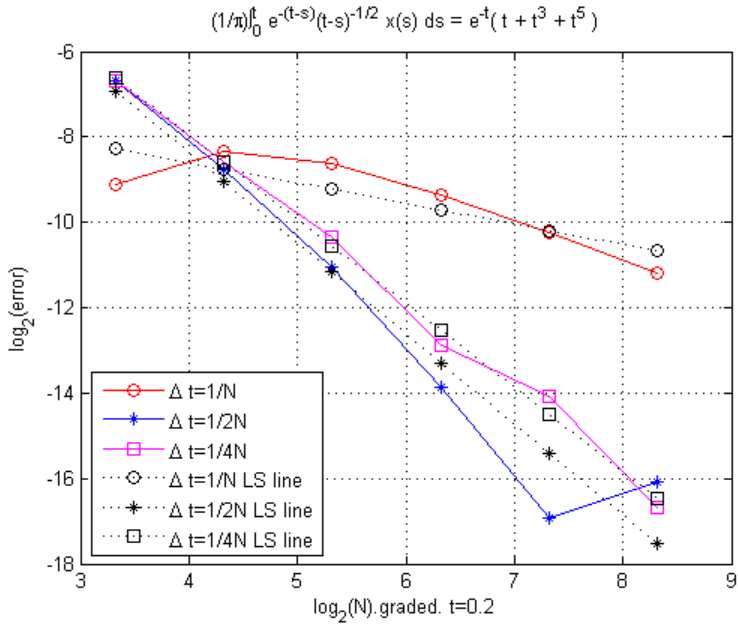

FIGURE 5. Example 4.6. Approximate rates of convergence with graded mesh at $t = 0.2$.

to $1/2N$, the rate increases to approximately 2.1 and then decreases to approximately 1.96 for $1/4N$. Figure 4 shows the approximate convergence rates at $t = 0.6$ to be 1.68, 1.86 and 1.66 for $\Delta t = 1/N, 1/2N$ and $1/4N$, respectively. In Figure 4, we see that the rate does not improve when we decrease the step-size at $t = 0.8$, where the convergence rates are approximately 1.95, 0.96 and 1.3 for $\Delta t = 1/N, 1/2N$ and $1/4N$, respectively. Although there were improvements at $t = 0.2$ and $t = 0.6$ with $\Delta t = 1/2N$, it was not as beneficial with $\Delta t = 1/4N$. There was no such improvement at $t = 0.8$.

Example 4.7. As a final application, we consider an example where the dependent variable, $x(t)$, also appears in the right side of the equation. Consider

$$\frac{d}{dt}\left(\int_{-1}^{0} \frac{x(t+s)}{|s|^{1/2}}\, ds\right) = x(t) - t^6 + \frac{1024}{231} t^{11/2}$$

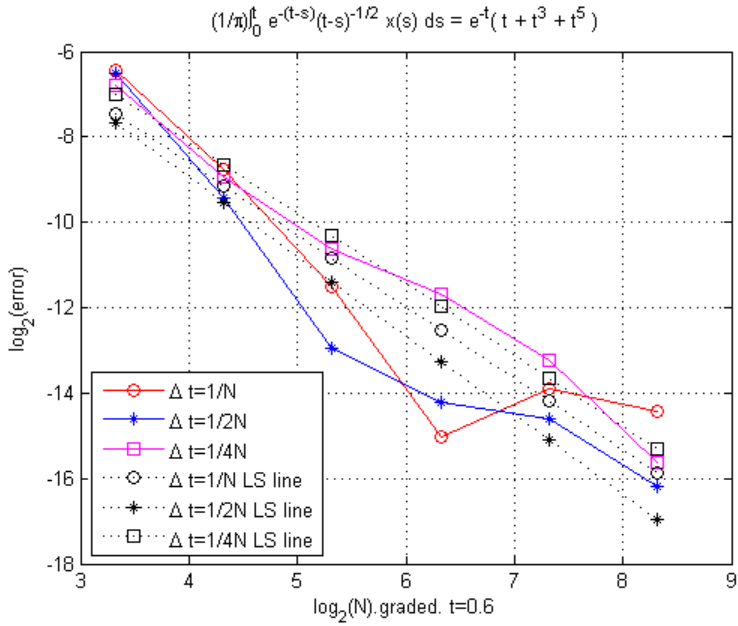

FIGURE 6. Example 4.6. Approximate rates of convergence with graded mesh at $t = 0.6$.

for $t > 0$ and $x(u) = 0$ for $u \leq 0$. The true solution is $x(t) = t^6$. This requires only a minor modification in the discretization of the boundary condition. More explicitly, if we recall the notation of Section 2, the discretized boundary condition (2.8) has the modified form $-\alpha_0^{k+1} + \sum_{j=1}^{N} g_j(\alpha_{j-1}^{k+1} - \alpha_j^{k+1})/\delta_j = f^{k+1}$. From Figure 6, we get a numerical convergence rate of about 1.5 for uniform mesh and 2 for graded mesh at time $t = 0.4$.

TABLE 9. Example 4.7. Uniform error table. $\Delta t = 1/N$.

mesh↓ time→	0.2	0.4	0.6	0.8
10	4.48E-05	0.001267769	0.008851268	0.035107414
20	1.86E-05	0.000504024	0.003454789	0.013542525
40	7.45E-06	0.000195381	0.001317837	0.005114189
80	2.89E-06	7.39E-05	0.000492225	0.001895588
160	1.10E-06	2.74E-05	0.000180854	0.000692665
320	4.07E-07	1.00E-05	6.57E-05	0.000250544

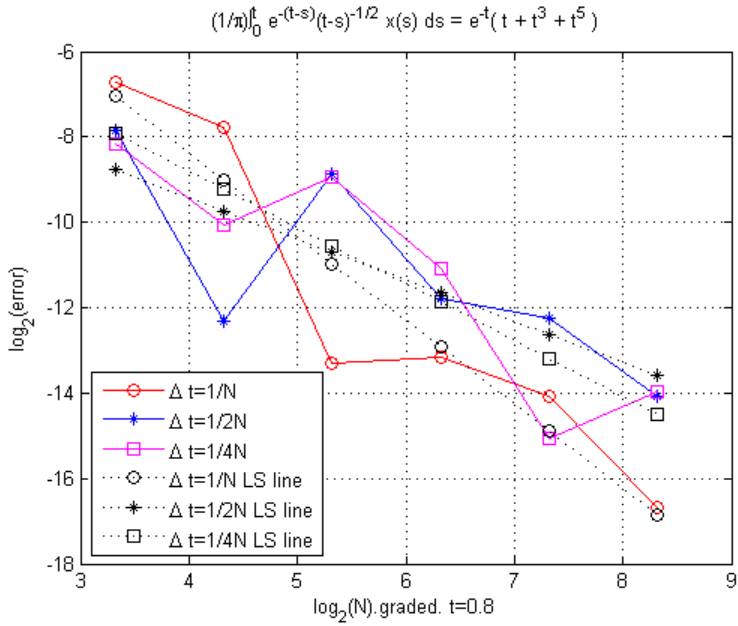

FIGURE 7. Example 4.6. Approximate rates of convergence with graded mesh at $t = 0.8$.

TABLE 10. Example 4.7. Graded error table. $\Delta t = 1/N$.

mesh↓ time→	0.2	0.4	0.6	0.8
10	2.28E-05	0.00046216	0.00271248	0.009714935
20	6.17E-06	0.00011739	0.000681765	0.002432978
40	1.57E-06	2.95E-05	0.000170666	0.000608517
80	3.94E-07	7.37E-06	4.27E-05	0.000152146
160	9.87E-08	1.84E-06	1.07E-05	3.80E-05
320	2.47E-08	4.61E-07	2.67E-06	9.51E-06

5. Conclusion. The "degradation" in the rate of convergence for SNFDEs with weakly singular kernels was observed in **[12]** (when using uniform meshes) and in this paper we investigated possible fixes of this phenomenon. In particular, we considered graded meshes (where grading was related to the strength of the singularity of the kernel

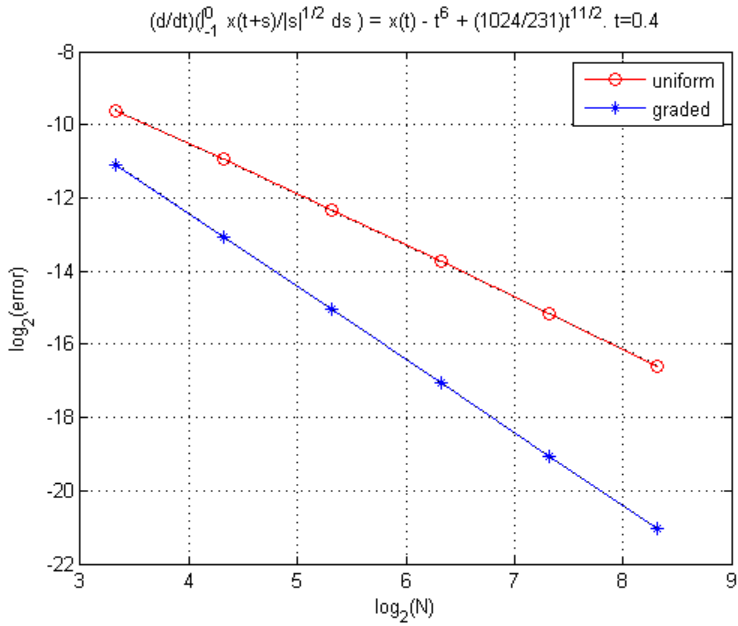

FIGURE 8. Example 4.7. Approximate rates of convergence for both meshes at $t = 0.4$.

function in the SNFDE under consideration) to improve on the rate of convergence. In Section 3, we established that the graded mesh is a viable alternative to uniform mesh and, in Section 4, we applied it to concrete examples. Examples 4.2 and 4.3 indeed show that the expected rate of convergence of 2 can be recovered if the graded mesh is applied. However, Examples 4.4 and 4.5 show that discontinuities in the derivatives of either the forcing function or the true solution may compromise the expected rates of convergence. Finally, in Example 4.7, we applied the scheme with graded mesh to a more general equation where we also observed an improvement in the convergence rate.

REFERENCES

1. H. Brunner, *Collocation methods for volterra integral and related functional differential equations*, Cambridge University Press, Cambridge, 2004.

2. _____, *The numerical solution of weakly singular Volterra integral equations by collocation on graded meshes*, Math. Comp. **45** (1985), 417-437.

3. J.A. Burns, E.M. Cliff and T.L. Herdman, *A state-space model for an aeroelastic system*, IEEE Conf. Dec. Contr., San Antonio, 1983.

4. J.A. Burns, T.L. Herdman and H.W. Stech, *Linear functional-differential equations as semigroups on product spaces*, SIAM J. Math. Anal. **14** (1983), 98-116.

5. J.A. Burns and K. Ito, *On well-posedness of integro-differential equations in weighted L^2-spaces*, Tech. Report No. 11-91, Center Appl. Math. Sci., University of Southern California, CA.

6. Y. Cao, G. Cerezo, T. Herdman and J. Turi, *Singularity expansion for a class of neutral equations*, J. Integral Equations Appl. **19** (2007), 13–32.

7. Y. Cao, T. Herdman and Y. Xu, *A hybrid collocation method for Volterra integral equations with weakly singular kernels*, SIAM J. Numer. Anal. **41** (2003), 364–381.

8. P.P.B. Eggermont, *A new analysis of the Euler-, midpoint- and trapezoidal-discretization methods for the numerical solution of Abel-type integral equations*, Med. Image Proc. Group Tech. Rep. No. MIPG34, State University of New York at Buffalo, Department of Computer Science, 1979.

9. R. Gorenflo and S. Vessella, S., *Abel integral equations*: *Analysis and applications*, Springer-Verlag, Berlin, 1991.

10. J.K. Hale and S.M.V. Lunel, *Introduction to functional differential equations*, Springer-Verlag, New York, 1993.

11. K. Ito, F. Kappel and J. Turi, *On well-posedness of singular neutral equations in the state space C*, J. Differential Eqs. **125** (1996), 40-72.

12. K. Ito and J. Turi, *Numerical methods for a class of singular integro-differential equations based on semigroup approximation*, SIAM J. Numer. Anal. **28** (1991), 1698-1722.

13. S. Jahanshahi, et al., *Solving Abel integral equations of first kind via fractional calculus*, J. King Saud Univ. Sci. **27** (2015), 161–167.

14. F. Kappel and K.P. Zhang, *On neutral functional-differential equations with nonatomic difference operator*, J. Math. Anal. Appl. **113** (1986), 311-343.

15. M.A. Rahman, M.S. Islam and M.M. Alam, *Numerical solutions of Volterra integral equations using Laguerre polynomials*, J. Sci. Res. **4** (2012), 357–364.

16. A.M. Wazwaz, *Linear and nonlinear integral equations*: *Methods and applications*, Springer, New York, 2011.

University of Texas at Dallas, Department of Mathematical Sciences, Richardson, TX 75080
Email address: **pxp122930@utdallas.edu**

University of Texas at Dallas, Department of Mathematical Sciences, Richardson, TX 75080
Email address: **turi@utdallas.edu**